Eur. Phys. J. A **13**, 297–305 (2002)

THE EUROPEAN PHYSICAL JOURNAL A

Development of magnetic rotation in light Gd nuclei; study of ^{142}Gd

R.M. Lieder[1,2,a], T. Rząca-Urban[2], H. Brands[1], W. Gast[1], H.M. Jäger[1], L. Mihailescu[1], Z. Marcinkowska[2], W. Urban[2], T. Morek[2], Ch. Droste[2], P. Szymański[2], S. Chmel[3], D. Bazzacco[4], G. Falconi[4], R. Menegazzo[4], S. Lunardi[4], C. Rossi Alvarez[4], G. de Angelis[5], E. Farnea[5], A. Gadea[5], D.R. Napoli[5], Z. Podolyak[5], Ts. Venkova[6], and R. Wyss[7]

[1] Institut für Kernphysik, Forschungszentrum Jülich, D-52425 Jülich, Germany
[2] Institute of Experimental Physics, University of Warsaw, PL-00-681 Warszawa, Poland
[3] Institut für Strahlen- und Kernphysik, University of Bonn, D-53115 Bonn
[4] Dipartimento di Fisica dell'Università and Istituto Nazionale di Fisica Nucleare, Sezione di Padova, I-35131 Padova, Italy
[5] Istituto Nazionale di Fisica Nucleare, Laboratori Nazionali di Legnaro, I-35020 Legnaro, Italy
[6] Institute of Nuclear Research and Nuclear Energy, Bulgarian Academy of Sciences, BG-1784 Sofia, Bulgaria
[7] Royal Institute of Technology, Physics Department Frescati, S-10405 Stockholm, Sweden

Received: 9 December 2001 / Revised version: 17 December 2001
Communicated by D. Schwalm

Abstract. High-spin states in ^{142}Gd have been populated by means of the ^{99}Ru(^{48}Ti, 2p3n) reaction at 240 MeV and investigated with the γ-spectrometer EUROBALL III and the charged-particle detector array ISIS. The features of four dipole bands have been determined and compared with tilted-axis cranking model calculations indicating that they are magnetic rotational bands. A transition from regular to irregular bands has been found approaching $N = 82$ demonstrating that this is a general phenomenon in nuclei near a double-shell closure.

PACS. 21.10.Re Collective levels – 21.60.Ev Collective models – 23.20.En Angular distribution and correlation measurements – 27.60.+j $90 \leq A \leq 149$

1 Introduction

A new type of rotation has been discovered in Pb nuclei around $A = 200$ [1–4]. The corresponding bands, following the $I(I+1)$ rule, consist of strong magnetic dipole transitions. These bands have been interpreted in the framework of the tilted-axis cranking (TAC) model as resulting from the coupling of the angular-momentum vectors of a few high-j particles of one kind and high-j holes of the other kind of nucleons, oriented approximately perpendicular to each other at the band head, for generating the total spin of the nucleus. This coupling results in a substantial component of the magnetic dipole moment which is transverse to the total spin [3]. As this component of the magnetic dipole moment rotates around the vector of the total angular momentum this new mode has been called "magnetic rotation" (MR) [5,6]. The angular momentum of the band is increased by the gradual alignment of the individual nucleon spins along the total angular-momentum vector. This way of angular-momentum production has been called "shears mechanism". The experimental evidence for the occurrence of MR bands is the appearance of regular sequences of magnetic dipole transitions. Their $B(M1)$ values are very large (several μ_N^2) and their crossover transitions, if existing at all, have very small $B(E2)$ values ($\approx 0.1\,(e\mathrm{b})^2$). Because of the alignment of the nucleon spin vectors with the total angular-momentum vector, the $B(M1)$ values are decreasing with increasing spin [7].

Magnetic rotations are not only expected in the Pb region but also for other regions close to magic numbers if high-j particles and holes are available and the deformation is small [5]. Also for the $N \approx 82$ region MR bands are expected and have indeed been observed, *e.g.* in ^{139}Sm [8]. A small prolate deformation has been assigned in the framework of TAC model calculations to the dipole band in ^{139}Sm [8]. For nuclei near a double-shell closure the sequences of dipole transitions may have excitation energies which do not follow anymore the $I(I+1)$ law. A transition from regular to irregular dipole bands has been observed in Cd, In and Sn nuclei with N approaching 50 (see [6] and references therein). This behaviour has been explained as a decrease of the quadrupole polarizability when the magic shell is approached [6]. In the immediate vicinity of doubly magic nuclei the short-range residual interactions between valence particles dominate which do not favour the formation of stable "shears blades". With present experimental possibilities this effect cannot be studied in the

[a] e-mail: r.lieder@fz-juelich.de

Pb region since high-spin states in nuclei close to ^{208}Pb cannot be populated. The heaviest Pb nucleus in which dipole bands have been found is ^{202}Pb [9,10]. A dipole band with an irregular level spacing has, however, been observed in ^{144}Gd [11] which neighbours the semi doubly magic nucleus ^{146}Gd. It has been interpreted as an oblate dipole band with a $\nu h_{11/2}^{-2}\pi h_{11/2}^{2}$ configuration [11]. It is, therefore, of interest to investigate whether more regular MR bands develop in the Gd nuclei with decreasing neutron number. In this report we present features of dipole bands in ^{142}Gd studied with EUROBALL III. Previous knowledge on the level scheme of ^{142}Gd results from investigations of Starzecki *et al.* [12] and Sugawara *et al.* [13].

2 Experimental methods

A study of high-spin states in the nucleus ^{142}Gd has been carried out with the γ-detector array EUROBALL III and the charged-particle detector array ISIS at the XTU tandem —linear accelerator (ALPI) combination of the Laboratori Nazionali di Legnaro, Italy. The EUROBALL III array was fully equipped with 15 CLUSTER detectors, 26 CLOVER detectors and 30 individual escape-suppressed Ge-detectors (tapered detectors) [14]. To populate high-spin states in ^{142}Gd the ^{99}Ru(^{48}Ti, 2p3n) reaction at a beam energy of 240 MeV has been used. The ^{99}Ru target, enriched to 95%, consisted of four self-supporting metal foils with a total thickness of 0.84 mg/cm^2. The recoil velocity was $v/c = 3.4\%$. In this reaction ^{142}Gd was populated with a maximum cross-section but neighbouring Tb, Gd, Eu and Sm nuclei were also populated strongly. In order to allow for an isotopic separation and to increase thus the selectivity of EUROBALL III the charged-particle detector array ISIS has been mounted in the center of the γ-detector array. The ISIS array [15] consisted of 40 Si particle telescopes with thicknesses of $\approx 140\,\mu$m and ≈ 1 mm for the ΔE and E detectors, respectively. Events were recorded when either ≥ 7 unsuppressed Ge-detectors fired or when ≥ 6 unsuppressed Ge-detectors and ISIS fired in coincidence. Approximately $4.5 \cdot 10^9$ high-fold γ-events have been collected, $\approx 60\%$ of which were associated with one or more detected particles. On average ≈ 4.5 γ-rays have been observed in an event after Compton suppression.

Cubes and matrices of various types have been sorted for the construction of the level scheme and for the determination of DCO and angular-distribution ratios as well as γ-ray polarization. The presort of the data and the sorting into γ-γ-γ cubes has been carried out with the software package "Ana" [16]. In the cube sort the composite detectors have been treated in the following way. Events from a CLUSTER detector were accepted i) when one Ge crystal fired, ii) when two neighbouring crystals fired or iii) when two neighbouring crystals and one non-neighbouring crystal fired. In cases ii) and iii) the energies of the neighbouring detectors were added up (addback mode). In case iii) the non-neighbouring detector was considered to have detected a second γ-ray from the target. Events from a CLOVER detector were accepted i) when one Ge crystal fired or ii) when two crystals fired in which case the energies were summed. From the ISIS data ΔE *vs.* E matrices were sorted to prepare banana gates for the various detected particles to be used in the cube sort. For the construction of the level scheme of ^{142}Gd, γ-γ-γ cubes gated by one and two protons, respectively, have been analysed. These cubes contain $\approx 48\%$ and $\approx 36\%$ of the events associated with ^{142}Gd but the latter cube is cleaner than the former one.

Directional correlation (DCO) and angular-distribution (AD) ratios and linear polarizations of γ-transitions in ^{142}Gd have been deduced from the EUROBALL data to establish their multipolarites and mixing ratios. An asymmetric angular-correlation matrix was sorted with the energies of the γ-rays measured with the CLOVER detectors (at 77° and 103° with respect to the beam direction) on one axis and of those observed with the most backward CLUSTER detectors (at 160°) and most forward tapered detectors (at 20°) on the other axis. Because thin targets have been used in the experiment the excited nuclei were recoiling into vacuum. For the long-lived states a disappearance of the alignment by deorientation was observed. Therefore, the angular distributions of γ-transitions below the $I = 10^+$ isomers (0.37 ns and 3.4 ns) and the 7^- isomer (0.14 ns) in ^{142}Gd [12,17] became fully isotropic. As result, two kind of angular correlations have been observed: i) directional correlations when both γ-rays were emitted from oriented states and ii) angular distributions (AD) when one γ-ray was emitted from an oriented state and the other one from a fully deoriented state. Appropriate DCO and angular-distribution ratios have been determined. Furthermore, to obtain a higher statistical accuracy for the AD ratios, two matrices have been sorted which both have the energies of the γ-rays observed with all detectors on one axis but on the other axis either those measured with the CLOVER detectors or those measured with the most backward CLUSTER detectors and most forward tapered detectors. Gating the matrices on the axes containing all detectors and taking into account the efficiencies of the different types of detectors allows to determine angular-distribution ratios, since the EUROBALL detectors are distributed over the full solid angle. The linear polarization of γ-transitions in ^{142}Gd was deduced using the CLOVER detectors working as polarimeters. Two γ-γ matrices: *vertical* (V) and *horizontal* (H) were sorted. The V (H) matrix contains the events in which one γ-quantum is Compton scattered in the direction perpendicular (parallel) to the emission plane [18] and registered in two segments of a CLOVER detector, whereas the second γ-ray was registered in any Ge-detector of EUROBALL. From the V and H matrices the number of perpendicular $N_\perp$ and parallel $N_\parallel$ scattered events were deduced, respectively. These quantities allow to determine the linear polarizations P of γ-rays [19]. The polarization sensitivity Q of the CLOVER detectors was taken from ref. [19].

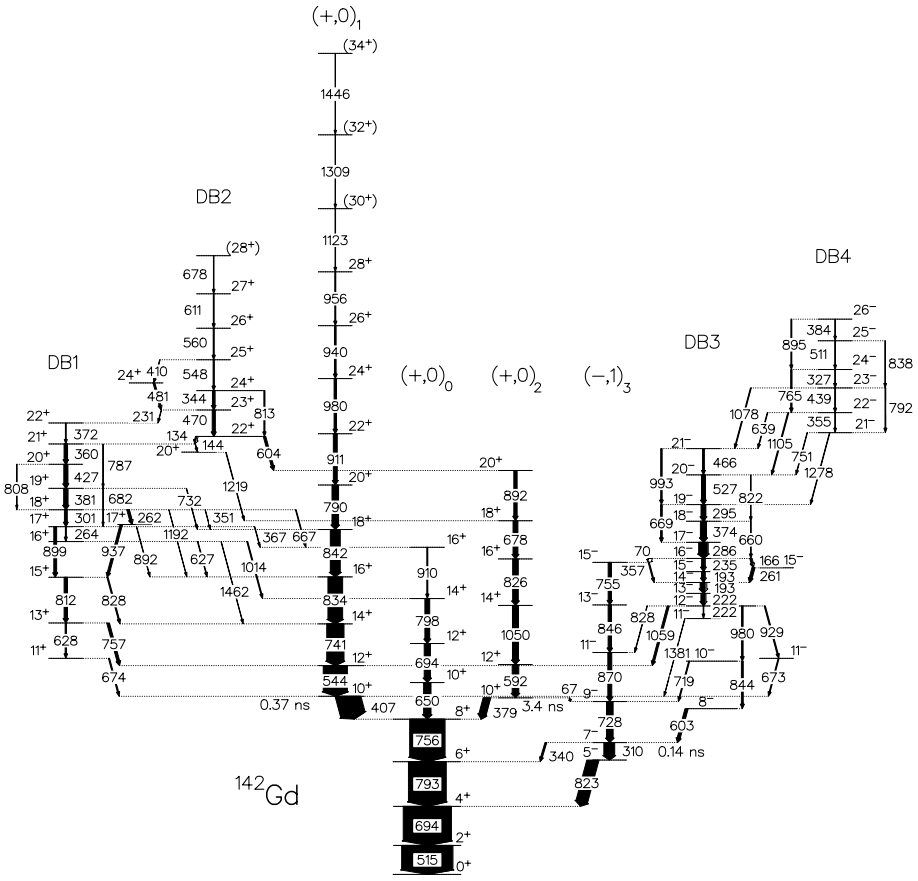

Fig. 1. Partial level scheme of ^{142}Gd. Uncertain spin-parity assignments are given in brackets. The widths of the arrows represent the intensities of the transitions.

3 Experimental results

A partial level scheme of ^{142}Gd resulting from the analysis of the EUROBALL III data is shown in fig. 1. It has been considerably extended in excitation energy and spin with respect to the schemes previously published [12,13]. In fig. 1 the dipole bands (denoted by DB and a number) and the bands into which they de-excite are shown. Spectra of the four dipole bands are shown in fig. 2. Table 1 contains spectroscopic information on the γ-ray transitions assigned to the dipole bands in ^{142}Gd. Spin-parity assignments result from angular distributions, DCO ratios, linear polarizations of γ-rays, conversion coefficients deduced from coincidence intensities as well as decay patterns. Results of the angular-distribution and linear-polarization analysis for stretched $E2$ transitions of the $(+,0)_1$ band and for members of the dipole bands DB1 and DB3 in ^{142}Gd are shown in fig. 3 in a plot of the polarization *vs.* the angular-distribution ratio. For comparison, fig. 3 contains also results of calculations for the used geometry, viz, for pure stretched $E1$ ($\Delta I = 1$) and $E2$ transitions ($\Delta I = 2$) and mixed $E2/M1$ transitions ($\Delta I = 1$) assuming a width of the Gaussian substate population distribution of $\sigma/I = 0.3$ (dashed curve and open stars) and 0.4 (solid curve and full stars). The $E2/M1$ curves represent the dependence of the polarization and angular-distribution ratio on the $E2/M1$ mixing ratio δ. To determine the linear polarization of the γ-rays belonging to DB1 and DB3 the statistics was improved by summing $N_\perp$ ($N_\parallel$) values obtained by gating on a few transitions placed below the transition of interest. From the data points for the stretched $E2$ transitions of 544, 741 and 834 keV in the $(+,0)_1$ band $\sigma/I = 0.4$ can be deduced. The data points for the dipole bands DB1 (301, 360, 381, 427 keV) and DB3 (286, 295, 374, 527 keV) are in agreement with the assignment of pure $M1$ or mixed $M1/E2$ character with $\delta \approx -0.1$. A pure stretched $E1$ character of these transitions can be excluded.

Four dipole bands have been observed in ^{142}Gd in the present work. From the previous work the existence of three of the dipole bands was known [13] but except for DB3 they were not well established. From the present high-statistics results, obtained with EUROBALL III, detailed information on the features of the dipole bands has been obtained. These results make a comparison with TAC model predictions feasible to find out whether the dipole bands can be interpreted as MR bands.

For DB1 the order of the transitions as well as the de-excitation pattern are different than previously proposed for dipole band (B) in ref. [13]. Three very weak crossover transitions have newly been identified. The $\Delta I = 1$ transi-

Table 1. Energies, intensities, branching ratios $\lambda = I_\gamma(E2)/I_\gamma(M1)$, $B(M1)/B(E2)$ ratios, angular-distribution ratios $R_{\rm AD}$ and polarizations P for transitions of the dipole bands in ^{142}Gd and for some de-exciting transitions used for spin assignments. The γ-ray intensities are normalized to $I_\gamma = 100$ for the $2^+ \to 0^+$ transition of 515.0 keV.

$I_{\rm i}^\pi$	$I_{\rm f}^\pi$	E_γ (keV)	I_γ	λ	$\frac{B(M1)}{B(E2)}$ $(\mu_N/e{\rm b})^2$	$R_{\rm AD}$ [a]	P
			Dipole band 1				
17^+	16^+	264.0 ± 0.3	1.5 ± 0.2			0.71 ± 0.17	
18^+	17^+	300.7 ± 0.2	5.0 ± 0.5			0.77 ± 0.10	−0.07 ± 0.19
19^+	18^+	381.1 ± 0.2	8.0 ± 0.8	0.024 ± 0.007	78 ± 22	0.84 ± 0.11	−0.12 ± 0.09
	17^+	682.1 ± 0.4	0.19 ± 0.05				
20^+	19^+	426.9 ± 0.2	7.6 ± 0.8	0.049 ± 0.012	63 ± 15	0.65 ± 0.07	−0.03 ± 0.16
	18^+	807.6 ± 0.7	0.37 ± 0.08				
21^+	20^+	360.4 ± 0.2	6.5 ± 0.8	0.072 ± 0.018	62 ± 15	0.61 ± 0.05	−0.33 ± 0.18
	19^+	787.4 ± 0.6	0.47 ± 0.10				
22^+	21^+	372.3 ± 0.3	1.5 ± 0.2			0.72 ± 0.17	
17^+	15^+	898.6 ± 0.2	5.6 ± 0.6			1.39 ± 0.10	
15^+	14^+	827.9 ± 0.3	2.3 ± 0.2			0.58 ± 0.14	
15^+	13^+	811.9 ± 0.3	6.7 ± 1.0			1.34 ± 0.10	
13^+	11^+	628.0 ± 0.2	2.6 ± 0.4			2.0 ± 1.0	
11^+	10^+	673.7 ± 0.5	2.1 ± 0.4			0.43 ± 0.13	
			Dipole band 2				
23^+	22^+	469.6 ± 0.2	4.4 ± 0.6			0.80 ± 0.10	
24^+	23^+	343.8 ± 0.2	3.6 ± 0.5	0.44 ± 0.08	13.7 ± 2.6	0.68 ± 0.10	
	22^+	812.9 ± 0.3	1.6 ± 0.2				
25^+	24^+	548.3 ± 0.4	1.8 ± 0.6			0.71 ± 0.10	
26^+	25^+	559.6 ± 0.4	1.5 ± 0.3			0.85 ± 0.10	
27^+	26^+	611.4 ± 0.2	1.2 ± 0.4			0.80 ± 0.10	
(28^+)	27^+	677.6 ± 0.5	0.8 ± 0.3				
22^+	21^+	133.9 ± 0.2	2.7 ± 0.3			0.83 ± 0.10	
			Dipole band 3				
12^-	11^-	222.0 ± 0.3	0.8 ± 0.1			0.69 ± 0.10	
13^-	12^-	222.3 ± 0.2	8.2 ± 1.4				
14^-	13^-	193.3 ± 0.3	11.6 ± 1.5			0.68 ± 0.06	
15^-	14^-	192.6 ± 0.3					
16^-	15^-	234.5 ± 0.2	6.1 ± 0.4			0.84 ± 0.15	
17^-	16^-	285.6 ± 0.2	17.0 ± 0.8			0.65 ± 0.06	−0.26 ± 0.12
18^-	17^-	374.4 ± 0.2	11.4 ± 0.6	0.13 ± 0.02	13.2 ± 2.0	0.55 ± 0.08	−0.14 ± 0.12
	16^-	660.2 ± 0.3	1.4 ± 0.2				
19^-	18^-	295.1 ± 0.2	8.7 ± 0.4	0.37 ± 0.04	9.9 ± 1.1	0.67 ± 0.10	−0.03 ± 0.15
	17^-	669.3 ± 0.2	3.2 ± 0.3				
20^-	19^-	527.0 ± 0.2	7.6 ± 0.4	0.12 ± 0.03	14.7 ± 3.4	0.73 ± 0.10	0.00 ± 0.18
	18^-	822.3 ± 0.4	0.9 ± 0.2				
21^-	20^-	466.4 ± 0.2	3.5 ± 0.4	0.79 ± 0.13	8.4 ± 1.4	0.52 ± 0.06	
	19^-	993.4 ± 0.2	2.8 ± 0.3			1.39 ± 0.08	
12^-	12^+	1058.7 ± 0.3	4.2 ± 0.6			1.30 ± 0.10	
						1.8 ± 0.4 [b]	
12^-	10^-	980.2 ± 0.3	3.0 ± 0.3			1.23 ± 0.10	
10^-	8^-	843.6 ± 0.2	3.6 ± 0.3			1.31 ± 0.06	
8^-	7^-	603.1 ± 0.2	6.0 ± 0.4			0.47 ± 0.10	

Table 1. Continued.

I_i^π	I_f^π	E_γ (keV)	I_γ	λ	$\frac{B(M1)}{B(E2)}$ $(\mu_N/\mathrm{eb})^2$	R_{AD} [a]	P
			Dipole band 4				
22^-	21^-	354.5 ± 0.3	0.8 ± 0.1				
23^-	22^-	438.6 ± 0.3	1.6 ± 0.2	0.9 ± 0.4	2.8 ± 1.2	0.70 ± 0.06	
	21^-	792.3 ± 1.0	1.5 ± 0.6				
24^-	23^-	326.5 ± 0.4	1.4 ± 0.4	1.9 ± 0.7	2.8 ± 1.0	0.67 ± 0.06	
	22^-	764.6 ± 0.3	2.6 ± 0.6			1.2 ± 0.1	
25^-	24^-	511.3 ± 0.4	1.2 ± 0.3	0.8 ± 0.3	2.6 ± 1.0		
	23^-	838.2 ± 0.3	1.0 ± 0.3				
26^-	25^-	384.4 ± 0.6	0.6 ± 0.1	3.0 ± 0.6	2.4 ± 0.5	0.63 ± 0.06	
	24^-	895.0 ± 0.3	1.8 ± 0.2			1.31 ± 0.10	
22^-	21^-	638.9 ± 0.3	1.1 ± 0.3			0.50 ± 0.08	
22^-	20^-	1104.6 ± 0.6	2.0 ± 0.3			1.4 ± 0.1	
23^-	21^-	1077.8 ± 0.3	1.7 ± 0.2			1.6 ± 0.2	
21^-	19^-	1277.8 ± 0.6	1.0 ± 0.2			1.5 ± 0.2	

[a] $R_{AD} \approx 0.81$ for pure stretched dipole transitions and $R_{AD} \approx 1.34$ for stretched quadrupole transitions for $\sigma/I = 0.4$ in the used geometry.
[b] DCO ratio obtained by gating on the 193 keV doublet; $R_{DCO}^{th} = 2.4 \pm 0.3$ for $\delta_{193} = -0.2 \pm 0.1$ and $\delta_{1059} = 0$.

tions have an $E2/M1$ mixing parameter of $\delta = -0.1 \pm 0.1$ (cf. fig. 3). The de-excitation is rather complex and proceeds to the $(+,0)_1$ and $(+,0)_0$ bands. The spin assignments result from the angular-distribution ratios of the 827.9 and 898.6 keV transitions connecting DB1 to the $(+,0)_1$ band. The latter one is a stretched quadrupole transition. The 827.9 keV transition is a $\Delta I = 1$ transition with an $E2/M1$ mixing ratio of $\delta = -0.2 \pm 0.2$. It is assumed that the spin of the level de-excited by the 827.9 keV transition is 15 and not 13, since otherwise a strong γ-ray to the 12^+ member of the $(+,0)_1$ band should exist but such a transition has not been observed. The angular-distribution ratios of the 673.7, 628.0 and 811.9 keV transitions are in agreement with this assignment, however the value of the 628.0 keV transition has a large uncertainty and the 673.7 keV transition is superimposed by a 673.2 keV stretched $E1$ transition of similar intensity. A positive parity was inferred considering that otherwise several of the transitions de-exciting DB1 would be $M2$ transitions competing with $E1$ transitions.

Six transitions and one crossover transition have been placed in DB2, whereas previously only two have been proposed for the corresponding dipole band (C) in ref. [13]. The excitation energy as well as the spin-parity assignments were fixed for DB2. This band de-excites into DB1 as well as into the $(+,0)_2$ band. The 133.9 keV transition to DB1 is a mixed $M1/E2$ transition considering its conversion coefficient of $\alpha_{tot} = 0.74 \pm 0.16$ ($\alpha_{tot}^{E1} = 0.13$, $\alpha_{tot}^{M1} = 0.89$, $\alpha_{tot}^{E2} = 0.87$). The angular-distribution ratio gives $\Delta I = 1$ and provides two solutions for the $E2/M1$ mixing ratio, viz, $\delta = 0.02 \pm 0.10$ and -10^{+6}_{-70}. For most of the cascade transitions in DB2 the angular-distribution ratios were determined confirming that they are of mixed dipole-quadrupole character with $\Delta I = 1$ having an $E2/M1$ mixing parameter of $\delta = 0.0 \pm 0.1$. Only one crossover transition has been found.

The DB3 agrees with the previously published dipole band (A) of ref. [13]. One cascade transition has been added at the lower end of the sequence and two additional crossover transitions have been found. The angular-distribution ratios and polarizations of the cascade transitions are as expected for a $\Delta I = 1$ sequence and give an $E2/M1$ mixing parameter of $\delta = -0.1 \pm 0.1$ (cf. fig. 3). The DB3 de-excites into the $(+,0)_1$ and $(-,1)_3$ bands. The spin assigments result from the angular-distribution ratio of the 603.1 keV transition and the DCO ratios of the 843.6 and 980.2 keV transitions connecting DB3 to the $(-,1)_3$ band. They give $\Delta I = 1$ for the first transition and stretched quadrupole character for the latter two. A decrease of the spin by 2 $\hbar$ can be excluded since the 356.8 keV transition de-exciting the 15^- level of the $(-,1)_3$ band into DB3 would then be a $M3$ transition. The angular distribution and DCO ratios of the 1058.7 keV transition are in agreement with a $\Delta I = 0$ assignment. From the conversion coefficient of the 70.0 keV transition of $\alpha_{tot} = 6.8 \pm 1.7$ ($\alpha_{tot}^{E1} = 0.8$, $\alpha_{tot}^{M1} = 5.7$, $\alpha_{tot}^{E2} = 9.5$) a negative parity was assigned to DB3. The band seems to terminate at $I^\pi = 21^-$ since the 466.4 keV transition is still fairly strong but no extension of DB3 has been found.

The new DB4 consists of five cascade and four crossover transitions. It de-excites in a complex way into DB3 and the proposed spin assignments are based on its de-excitation and on the DCO and AD ratios obtained for most of the in-band and connecting transitions. For the

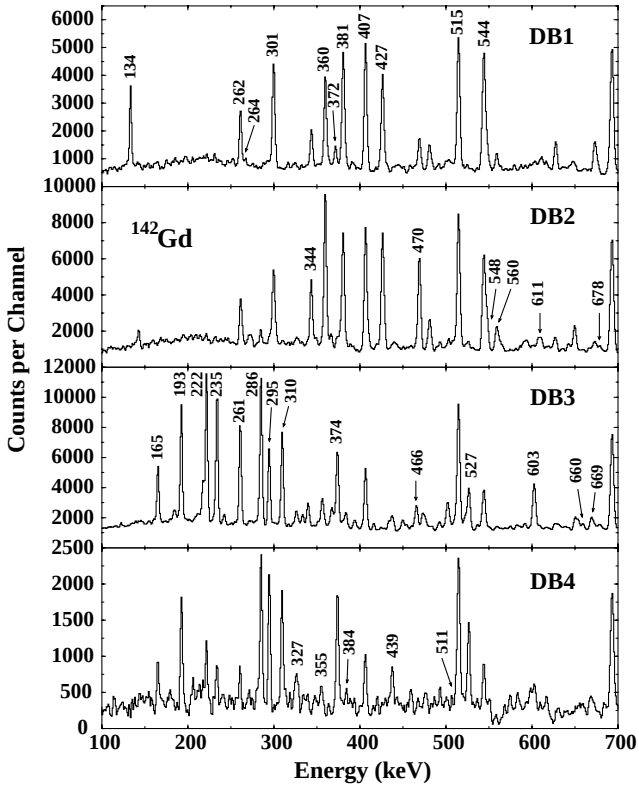

Fig. 2. Spectra of the dipole bands in ^{142}Gd. The energies of the in-band transitions and of a few low-spin transitions are given in keV. Double gates have been placed on the following transitions to create the spectra: DB1: 812 – (407 + 515 + 756 + 793), DB2: 134 – (407 + 515 + 544 + 694 + 756 + 793), DB3: 193 – (310 + 515 + 694 + 823) and DB4: 1278 – (286 + 295 + 374) and 1105 – (286 + 295 + 374 + 527).

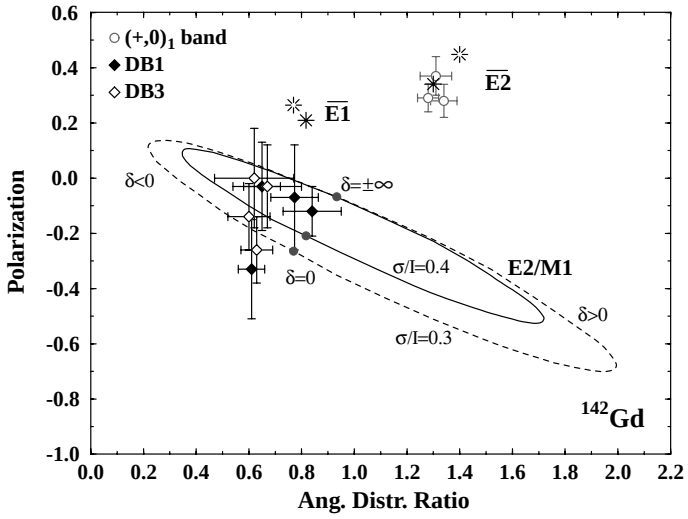

Fig. 3. Polarization P *vs.* angular-distribution ratio for the $(+,0)_1$ band and the dipole bands DB1 and DB3 in ^{142}Gd. Theoretical values are shown for pure stretched $E1$ and $E2$ transitions (denoted as $\overline{E1}$ and $\overline{E2}$, respectively) and for mixed $E2/M1$ transitions ($\Delta I = 1$) as a function of the mixing ratio δ for two values of the width of the Gaussian substate population distribution σ/I. For pure $E1$ and $E2$ transitions full and open stars correspond to $\sigma/I = 0.4$ and 0.3, respectively.

$\Delta I = 1$ transitions of DB4 an $E2/M1$ mixing parameter of $\delta = -0.1 \pm 0.1$ was found. For the proposed spin assignment a negative parity is appropriate since otherwise $M2$ and $E1$ transitions would have to compete.

4 Discussion

To find out whether the dipole bands DB1–DB4 in ^{142}Gd can be interpreted as MR bands, their features have been compared with predictions of TAC model calculations as well as calculations using the semiclassical vector model of Frauendorf and Dönau [20,21]. The angular momentum as a function of the rotational frequency is shown in fig. 4 for these bands. In this representation the dipole bands appear to be fairly regular, although the transition energies do not increase regularly with spin, because the rotational frequencies are calculated from $\Delta I = 2$ energy differences. Figure 4 suggests that DB2 originates from DB1 and DB4 from DB3, respectively, through band crossing. The alignment gain is in both cases $\approx 4\hbar$. The increase of the alignment in the beginning of DB3 may indicate that the low-spin members of this cascade have a different structure than the levels with $I \geq 15$. The $B(M1)/B(E2)$ ratios could be deduced whenever crossover transitions were observed and are shown as a function of spin in fig. 5. For DB1 values of $B(M1)/B(E2) \geq 60\,(\mu_N/e\mathrm{b})^2$ have been found which are in the order of magnitude expected for MR bands. The $B(M1)/B(E2)$ ratio of DB2 is by a factor of ≈ 5 smaller. For DB3 values of $B(M1)/B(E2) \approx 10\ (\mu_N/e\mathrm{b})^2$ have been observed and the values for DB4 are by a factor of ≈ 4 smaller. The observation, that the changes in angular momenta and $B(M1)/B(E2)$ ratios are similar for the pairs of dipole bands DB1–DB2 and DB3–DB4 may indicate that the same nucleon pair is aligning in both cases.

The dipole bands in ^{142}Gd can be associated with a small oblate deformation of the nucleus. TRS calculations show minima for the deformation parameters $\varepsilon_2 \approx 0.15$ and $\gamma \approx -60°$ for a frequency range of $0.2 \leq \hbar\omega \leq 0.5$ MeV. The minima are rather shallow, indicating a γ-softness. For this deformation the $h_{11/2}$ neutron-hole and $g_{7/2}$ proton-hole states with small Ω values and the $h_{11/2}$ proton states with large Ω values contribute to the configurations of the dipole bands. A $\nu h_{11/2}^{-2}\pi h_{11/2}^{2}$ configuration may be assigned to DB1 and a $\nu h_{11/2}^{-2}\pi h_{11/2}^{1} g_{7/2}^{-1}$ configuration to DB3. The bands DB2 and DB4 likely result from the breakup of a second $h_{11/2}$ neutron-hole pair. Considering an alignment of the spins of the hole states along the rotation axis and of the particle states along the symmetry axis (Fermi-aligned coupling scheme), angular momenta of 14 and 15 $\hbar$, respectively, are expected for the lowest members of DB1 and DB3. In the level scheme of fig. 1 the dipole band DB1 starts with $I = 16$ and DB3 with $I = 11$, indicating that the first transitions of

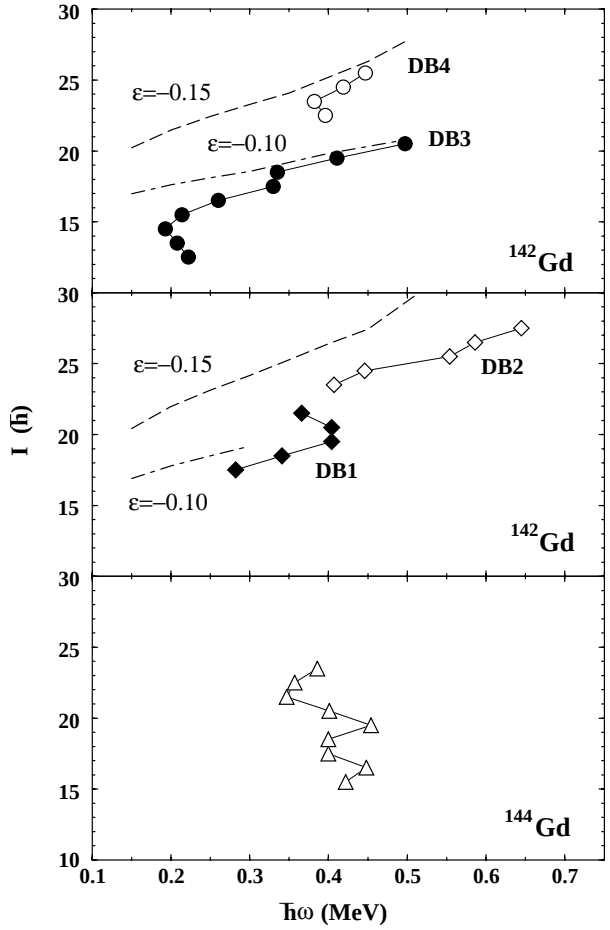

Fig. 4. Angular momentum *vs.* rotational frequency for the dipole bands in ^{142}Gd. The thin lines connect the data points. The broken lines result from TAC model calculations. For comparison also the dipole band in ^{144}Gd is shown.

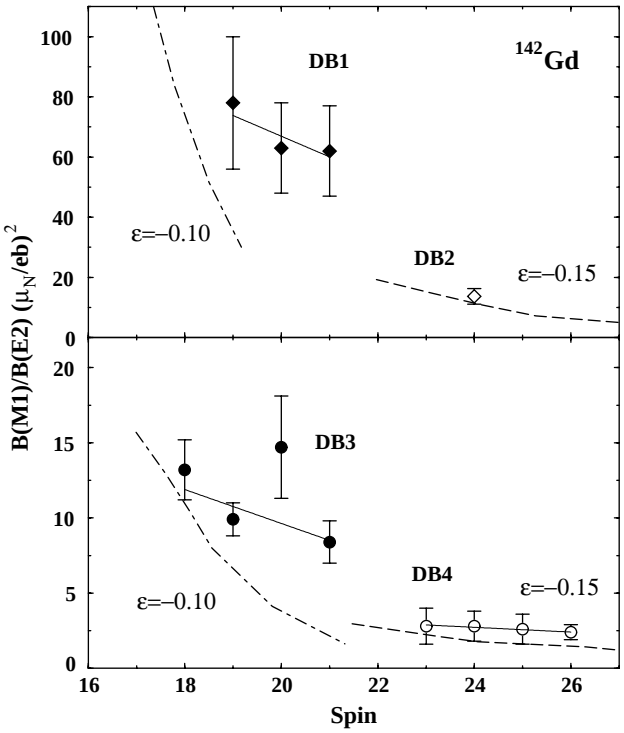

Fig. 5. $B(M1)/B(E2)$ ratio *vs.* spin for the dipole bands in ^{142}Gd. The thin lines result from fits of straight lines to the data points. The broken lines result from TAC model calculations.

the latter band result from a different configuration. The alignment of a second $h_{11/2}$ neutron-hole pair gives an alignment gain of $\approx 5\ \hbar$ similar to the observed value.

The large $B(M1)/B(E2)$ ratios for some of the dipole bands in ^{142}Gd are comparable to those of other regions of MR. For a more detailed investigation of the features of these bands they have been compared with predictions of TAC model calculations as well as of the semiclassical Frauendorf and Dönau formula [20,21] assuming the above-proposed configurations.

The formulas to calculate $B(M1)/B(E2)$ ratios developed by Frauendorf and Dönau [20,21] in the framework of a semiclassical vector model have been used in the following form:

$$B(M1) = \frac{3}{8\pi}\left[(g_\pi - g_\mathrm{R})K_\pi\sqrt{1-\frac{K^2}{I^2}} - (g_\nu - g_\mathrm{R})i_\nu\frac{K}{I}\right]^2 \quad (1)$$

obtained assuming that the neutrons are aligned along the rotation axis, $K_\nu = 0$, and the protons along the symmetry axis, $i_\pi = 0$.

$$B(E2) = \frac{5}{16\pi}\,Q_0^2\langle I\,K\,2\,0\,|I{-}2\,K\rangle^2\,. \quad (2)$$

Calculations have been carried out for DB1 and DB2 since the g-factors of the $\nu h_{11/2}^{-2}$ and $\pi h_{11/2}^2$ configurations have been measured as $g_\nu = -0.18 \pm 0.02$ for ^{140}Sm [22] and $g_\pi = 1.27{\pm}0.09$ for ^{140}Sm [22] as well as $g_\pi = 1.6{\pm}0.4$ for ^{142}Gd [23]. For g_π the former value has been utilized as it is more precise. For the quadrupole moment the value $Q = -1.46 \pm 0.1\ e$b has been used which was measured for the $\pi h_{11/2}^2$ isomer in ^{144}Gd representing a deformation of $\varepsilon_2 \approx -0.1$ [24,25]. It was transformed into the intrinsic quadrupole moment Q_0 using the equation $Q = I(2I-1)/[(I+1)(2I+3)]\,Q_0$. For the rotational g-factor $g_\mathrm{R} = Z/A = 0.45$ has been assumed, however, the dependence of the $B(M1)/B(E2)$ ratios on g_R is small. The calculated $B(M1)/B(E2)$ ratios for $K = K_\pi = 10$ and $i_\nu = 10$ for DB1 and $i_\nu = 16$ for DB2 are compared in table 2 with the experimental values. It can be seen that the calculated $B(M1)/B(E2)$ ratios for DB1 and DB2 are, respectively, about 3 and 13 times larger than the experimental values indicating that collective rotation is an unlikely explanation for these dipole bands in ^{142}Gd. For DB3 and DB4 no calculations of this type have been carried out since the g-factors of the considered configurations are not known.

Table 2. Comparison of experimental $B(M1)/B(E2)$ ratios, with values calculated in the framework of the semiclassical vector model of Frauendorf and Dönau (FD calc.).

Band	I_i^π	$\frac{B(M1)}{B(E2)}$ $(\mu_N/\mathrm{eb})^2$	
		Exp.	FD calc.
DB1	18^+		210
	19^+	78 ± 22	188
	20^+	63 ± 15	172
	21^+	62 ± 15	159
	22^+		149
DB2	24^+	13.7 ± 2.6	178
	25^+		169
	26^+		160
	27^+		153
	(28^+)		147

The parameter κ of the QQ interaction used in the TAC model calculations is scaled from the Pb region according to $\kappa \propto A^{-5/3}$. Pairing is taken into account by using gap energies of $\Delta_\pi = 0.92$ and $\Delta_\nu = 1.04$ MeV as deduced from odd-even mass differences. The chemical potentials were chosen to reproduce the particle numbers. The quadrupole deformation parameter has been varied from $\varepsilon_2 = -0.10$ to -0.15 with $\varepsilon_4 = 0$. For simplicity an axially symmetric deformation has been used. The results of the TAC model calculations for DB1 and DB3 using $\varepsilon_2 = -0.10$ and for DB2 and DB4 using $\varepsilon_2 = -0.15$ are included in figs. 4 and 5. It is expected that the alignment of a second $\nu h_{11/2}$ hole pair causes an increase of the deformation suggesting that the deformation for DB2 and DB4 is larger than for DB1 and DB3. The angular-momentum curves have similar slopes as the experimental curves but lie $\approx 1\ \hbar$ above them for DB1, DB3 and DB4 and $\approx 3\ \hbar$ for DB2 (cf. fig. 4) which can be considered as a good agreement since the angular momenta are generally somewhat overestimated by the TAC model. However, it should be mentioned that for DB1 and DB2 the appropriate configurations could in the calculations not be followed until the largest observed rotational frequencies because of the increased level density and the presence of many crossings of the orbitals. The irregularities in the experimental angular-momentum curves may indicate that the shears blades are not completely stretched over the whole frequency range. The experimental $B(M1)/B(E2)$ ratios of DB1–DB4 are overall reproduced reasonably well, although the calculated slope of DB1 is considerably larger than the observed one (cf. fig. 5). The agreement between experiment and calculation suggests that the dipole bands DB1–DB4 in ^{142}Gd can be interpreted as MR bands.

A dipole band has also been observed in ^{144}Gd [11]. It has been interpreted as an oblate dipole band with a $\nu h_{11/2}^{-2}\pi h_{11/2}^2$ configuration for the lowest band members. The same configuration has been assigned to DB1 in ^{142}Gd and DB2 results from the alignment of a second $h_{11/2}$ neutron-hole pair. Therefore, the angular momenta as a function of the rotational frequency of these bands have been compared in fig. 4. The dipole band in ^{144}Gd shows a much less regular behaviour than DB1 and DB2 in ^{142}Gd since I increases within a narrow frequency range of ≈ 0.1 MeV. This behaviour reflects the irregular level spacings in this band and is probably due to configuration changes [11]. With increasing frequency it becomes more favourable to move protons from the $d_{5/2}$ or $g_{7/2}$ into the $h_{11/2}$ orbitals. These particle-hole excitations will increase the alignment of the dipole sequence. One can classify the different proton excitations in terms of $(\pi h_{11/2})^x \otimes (\pi g_{7/2}/d_{5/2})^{-x}$ configurations [11].

The transition from irregular dipole bands in ^{144}Gd to more regular ones in ^{142}Gd results from an increase of the distance to the semi doubly magic nucleus ^{146}Gd. The present results show that this effect is not a unique feature of the light Cd, In and Sn nuclei [6] but a more general phenomenon. An increased quadrupole polarizability is required to produce the more regular dipole bands in ^{142}Gd. The deformation induced by the active particles and holes aligns their angular momenta into two stable blades forming the shears. In ^{144}Gd short-range residual interactions between valence particles dominate which are not able to stabilize the blades. The spins of the particles and holes contributing to the configuration of the dipole cascade change their orientation with respect to each other so that the blades of the shears are not anymore stretched [6]. A deformation change between ^{142,144}Gd is also clearly visible for their low-spin states. In ^{142}Gd a ground-state sequence and collective sequences based on the isomers are observed which have structures typical for a rotor with a modest deformation. In contrast, ^{144}Gd [11] shows up to a spin of $I \approx 18$ a structure which requires an explanation in terms of shell-model excitations as expected since the shell closure at $N = 82$ is approached. The transition from deformed to spherical-like structures appears to occur rather suddenly between $N = 78$ and 80.

5 Conclusions

A detailed investigation of the features of four dipole bands in ^{142}Gd has been carried out with EUROBALL III. They show the typical characteristics of MR bands, viz, a fairly regular increase of the angular momentum with the rotational frequency and the observation of strong $M1$ and weak crossover $E2$ transitions with $B(M1)/B(E2)$ ratios up to 60 $(\mu_N/\mathrm{eb})^2$. A $\nu h_{11/2}^{-2}\pi h_{11/2}^2$ configuration has been assigned to DB1 and a $\nu h_{11/2}^{-2}\pi h_{11/2}^1 g_{7/2}^{-1}$ configuration to DB3. The bands DB2 and DB4 are considered to originate from DB1 and DB3, respectively, through band crossings due to the breakup of a second $h_{11/2}$ neutron-hole pair. These features are reasonably well reproduced by TAC model calculations. On the other hand, calculations of the $B(M1)/B(E2)$ ratios for DB1 and DB2 using the semiclassical vector model of Frauendorf and Dönau show that the experimental values are strongly overestimated indicating that the bands do not represent collective rotations. Therefore, the dipole bands may be interpreted as MR

bands. A transition from irregular dipole bands in ^{144}Gd to more regular ones in ^{142}Gd is found which reflects an increase of the distance to the semi doubly magic nucleus ^{146}Gd. An increased quadrupole polarizability is required to produce regular dipole bands. With the present experimental possibilities the transition from regular to irregular dipole bands cannot be investigated in the Pb region. Our results for ^{142,144}Gd show, however, that a transition from irregular to regular dipole bands is not a unique feature of the light Cd, In and Sn nuclei but a more general phenomenon.

We are very grateful to H.J. Maier, Sektion Physik, Universität München, for the production of the self-supporting ^{99}Ru foils. We are indepted to the technical staff of the Tandem XTU and ALPI accelerator combination of the Laboratori Nazionali di Legnaro for providing the beam. We want to thank M. Pracharz for assistance in the data analysis. We acknowledge enlightening discussions on the interpretation with S. Frauendorf. The work was in part funded by the EU under the contract ERBFMRXCT970123, by the Volkswagen Foundation under the contract number I/71 976 and by the KBN Grant No. 5P03B 084 20. A Humboldt Research Fellowship by the Foundation for Polish Science is gratefully acknowledged (R.M.L.).

References

1. H. Hübel, G. Baldsiefen, R.M. Clark, S.J. Asztalos, J.A. Becker, L. Bernstein, M.A. Deleplanque, R.M. Diamond, P. Fallon, I.M. Hibbert, R. Krücken, I.Y. Lee, A.O. Macchiavelli, R.W. MacLeod, G. Schmid, F.S. Stephens, K. Vetter, R. Wadsworth, Z. Phys. A **358**, 237 (1997).
2. S. Chmel, F. Brandolini, R.V. Ribas, G. Baldsiefen, A. Görgen, M. De Poli, P. Pavan, H. Hübel, Phys. Rev. Lett. **79**, 2002 (1997).
3. R.M. Clark, S.J. Asztalos, G. Baldsiefen, J.A. Becker, L. Bernstein, M.A. Deleplanque, R.M. Diamond, P. Fallon, I.M. Hibbert, H. Hübel, R. Krücken, I.Y. Lee, A.O. Macchiavelli, R.W. MacLeod, G. Schmid, F.S. Stephens, K. Vetter, R. Wadsworth, S. Frauendorf, Phys. Rev. Lett. **78**, 1868 (1997).
4. R.M. Clark, A.O. Macchiavelli, Annu. Rev. Nucl. Part. Sci. **50**, 1 (2000).
5. S. Frauendorf, Z. Phys. A **358**, 163 (1997).
6. S. Frauendorf, Rev. Mod. Phys. **73**, 463 (2001).
7. R.M. Clark, R. Krücken, S.J. Asztalos, J.A. Becker, B. Busse, S. Chmel, M.A. Deleplanque, R.M. Diamond, P. Fallon, D. Jenkins, K. Hauschild, I.M. Hibbert, H. Hübel, I.Y. Lee, A.O. Macchiavelli, R.W. MacLeod, G. Schmid, F.S. Stephens, U.J. van Severen, K. Vetter, R. Wadsworth, S. Wan, Phys. Lett. B **440**, 251 (1998).
8. F. Brandolini, M. Ionescu-Bujor, N.H. Medina, R.V. Ribas, D. Bazzacco, M. De Poli, P. Pavan, C. Rossi Alvarez, G. de Angelis, S. Lunardi, D. De Acuña, D.R. Napoli, S. Frauendorf, Phys. Lett. B **338**, 468 (1996).
9. G. Baldsiefen, P. Maagh, H. Hübel, W. Korten, S. Chmel, M. Neffgen, W. Pohler, H. Grawe, K.H. Maier, K. Spohr, R. Schubart, S. Frauendorf, H.J. Maier, Nucl. Phys. A **592**, 365 (1995).
10. A. Görgen, H. Hübel, D. Ward, S. Chmel, R.M. Clark, M. Cromaz, R.M. Diamond, P. Fallon, K. Hauschild, G.J. Lane, I.Y. Lee, A.O. Macchiavelli, K. Vetter, Eur. Phys. J. A **9**, 161 (2000).
11. T. Rząca-Urban, S. Utzelmann, K. Strähle, R.M. Lieder, W. Gast, A. Georgiev, D. Kutchin, G. Marti, K. Spohr, P. von Brentano, J. Eberth, A. Dewald, J. Theuerkauf, I. Wiedenhöfer, K.O. Zell, K.H. Maier, H. Grawe, J. Heese, H. Kluge, W. Urban , R. Wyss, Nucl. Phys. A **579**, 319 (1994).
12. W. Starzecki, G. de Angelis, B. Rubio, J. Styczen, K. Zuber, H. Güven, W. Urban, W. Gast, P. Kleinheinz, S. Lunardi, F. Soramel, A. Facco, C. Signorini, M. Morando, W. Męczynski, A.M. Stefanini, G. Fortuna, Phys. Lett. B **200**, 419 (1988).
13. M. Sugawara, H. Kusakari, Y. Igari, K. Terui, K. Myojin, D. Nishimiya, S. Mitarai, M. Oshima, T. Hayakawa, M. Kidera, K. Furutaka, Y. Hatsukawa, Z. Phys. A **358**, 1 (1997).
14. R.M. Lieder, in *Experimental Techniques in Nuclear Physics*, edited by D.N. Poenaru, W. Greiner (Walter de Gruyter, Berlin, 1997) p. 137.
15. E. Farnea, G. de Angelis, M. de Poli, D. De Acuña, A. Gadea, D.R. Napoli, P. Spolaore, A. Buscemi, R. Zanon, R. Isocrate, D. Bazzacco, C. Rossi-Alvarez, P. Pavan, A.M. Bizzeti-Sona, P.G. Bizzeti, Nucl. Instrum. Methods A **400**, 87 (1997).
16. W. Urban, Manchester University, Nuclear Physics Report 1991-1992, p. 95.
17. *Table of Isotopes*, 8th edition (Wiley, 1996).
18. Ch. Droste, S.G. Rohozinski, K. Starosta, T. Morek, J. Srebrny, P. Magierski, Nucl. Instrum. Methods A **378**, 518 (1996).
19. K. Starosta, T. Morek, Ch. Droste, S.G. Rohozinski, J. Srebrny, A. Wierzchucka, M. Bergström, B. Herskind, E. Melby, T. Czosnyka, P.J. Napiorkowski, Nucl. Instrum. Methods A **423**, 16 (1999).
20. F. Dönau, S. Frauendorf, *Proceedings of the Conference on High Angular Momentum Properties of Nuclei, Oak Ridge, 1982*, edited by N.R. Johnson (Harwood Academic Publishers, Chur, 1983) p. 143.
21. F. Dönau, Nucl. Phys. A **471**, 469 (1987).
22. D. Bazzacco, F. Brandolini, K. Loewenich, S. Lunardi, P. Pavan, C. Rossi Alvarez, F. Soramel, M. De Poli, A.M.I. Haque, G. de Angelis, Phys. Lett. B **206**, 404 (1988).
23. D. Bazzacco, F. Brandolini, K. Loewenich, P. Pavan, C. Rossi Alvarez, F. Soramel, M. De Poli, A.M.I. Haque, Annual Report 1987, No. LNL-INFN (REP)-014/88, 1988, p. 7.
24. O. Häusser, P. Taras, W. Trautman, D. Ward, T.K. Alexander, H.R. Andrews, B. Haas, D. Horn, Nucl. Phys. A **379**, 287 (1982).
25. E. Dafni, J. Bendahan, C. Broude, G. Goldring, M. Hass, E. Naim, M.H. Rafailovich, C. Chasman, O.C. Kistner, S. Vajda, Phys. Rev. Lett. **53**, 2473 (1984).